

# Multiclass Anomaly Detection in GI Endoscopic Images using Optimized Deep One-class Classification in an Imbalanced Dataset

Mohammad Reza Mohebbian, Seyed Shahim Vedaiei, Khan A. Wahid and Paul Babyn

M.R. Mohebbian, S.S. Vedaiei, K.A. Wahid, are with Department of Electrical and Computer Engineering, University of Saskatchewan, Saskatoon, SK S7N 5A9, Canada.

P.Babyn is with Saskatchewan Health Authority, Saskatoon, SK S7K 0M7, Canada.

**Abstract**— Wireless Capsule Endoscopy helps physicians examine the gastrointestinal (GI) tract noninvasively, with the cost of generating many images. Many available datasets, such as KID2 and Kvasir, suffer from imbalance issue which make it difficult to train an effective artificial intelligence (AI) system. Moreover, increasing number of classes makes the problem worse. In this study, an ensemble of one-class classifiers is used for detecting anomaly. This method focuses on learning single models using samples from only one class, and ensemble all models for multiclass classification. A total of 1,778 normal, 227 inflammation, 303 vascular diseases, and 44 polyp images have been used from the KID2 dataset. In the first step, deep features are extracted based on an autoencoder architecture from the preprocessed images. Then, these features are oversampled using Synthetic Minority Over-sampling Technique and clustered using Ordering Points to Identify the Clustering Structure. To create one-class classification model, the Support Vector Data Descriptions are trained on each cluster with the help of Ant Colony Optimization, which is also used for tuning clustering parameters for improving F1-score. This process is applied on each classes and ensemble of final models used for multiclass classification. The entire algorithm ran 5 times and obtained F1-score  $96.3 \pm 0.2\%$  and macro-average F1-score  $85.0 \pm 0.4\%$ , for anomaly detection and multiclass classification, respectively. The results are compared with GoogleNet, AlexNet, Resnet50, VGG16 and other published algorithms, and demonstrate that the proposed method is a competitive choice for multiclass class anomaly detection in GI images.

**Index Terms**—Endoscopy, one-class classification, ant colony optimization, deep feature

## 1. INTRODUCTION

Endoscopy is a gold standard for Gastrointestinal (GI) tract examination and essential for early detection of GI diseases [1]. All traditional endoscopy methods, such as colonoscopy and gastroscopy, are invasive but they provide real-time video examination and can visualize various disorders, including polyposis syndromes, esophagitis, and ulcerative colitis [2]. On the other hand, Wireless Capsule Endoscopy (WCE) provides a noninvasive way for GI imaging of regions that were not accessible using traditional methods, and is less painful for the patients [3]. Here, a physician analyzes the recorded video. The number of GI images that are examined to find suspected abnormalities is enormous and requires substantial attention and time of the physician.

The early-stage disease is typically associated with polyps and mucosal inflammation. Research reveals that the accuracy of gastroenterologists diagnosing of small polyp (less than 1 cm) is roughly 76% [4]. On the other hand, the inflammatory process, including the accumulation of immune cells, affects the natural structure and composition of the gastrointestinal tract. Crohn's disease (CD) is a subset of the Inflammatory Bowel Disease category that involves ulcerative colitis [5]. Mucosal breaks, like ulcers, are the most frequent anomalies found in the small bowel [6]. Over the past years, inflammation treatment techniques have changed from simplistic symptoms management to near supervision of mucosal inflammation, and personalized monitoring [7]. Therefore, using a computer-aided diagnosis system with image processing and machine-learning algorithms may save cost and time as well as help to reduce human errors [8].

We organize the literature into three groups for anomaly detection:

- There are various researches in the literature that target specific anomaly detection (binary

classification). The majority of the published research in endoscopy comes from this category. Li and Meng [9] demonstrated that a mix of color and texture features is more effective for accurately describing polyps than any color or texture feature alone. Bernal *et al.* [10] used inpainting diffusion algorithm combined with an energy map for polyp detection on a publicly available dataset [11] and acquired 84.2% accuracy. Zhou *et al.* (Zhou et al., 2014) utilized variance of color channels with SVM for polyp detection on a private dataset and could achieve 90.7% accuracy. Another private dataset is used by Klare *et al.* [12], wherein they used a software named APDS for polyp identification. They evaluated results by endoscopists and reported 85.3% accuracy. Hassan *et al.* also used private dataset and another software for polyp detection, called Medtronic software, and could achieve 82% accuracy. Ševo *et al.* (Ševo et al., 2016) were used a private dataset for inflammatory detection. They used edge and texture analysis and evaluated their method on external dataset and achieved 84% accuracy. Gulati *et al.* [13] used convolutional neural network (CNN) and achieved 90 % recall and 63 % specificity for polyp identification. Zhang *et al.* [14] applied Transfer learning for feature extraction on a private dataset and used SVM for polyp detection which achieved 85.9% accuracy and 87% F1-score. The KID1 dataset [15] is utilized by Georgakopoulos *et al.* [16] for inflammatory detection. They used a Convolutional Neural Network (CNN) architecture and achieved 90.2% accuracy.

- There are some research aim to detect anomaly in general concept (binary classification). Jain *et al.* [17] combined KID1 and KID2 and used random forest-based ensemble classifier with fractal features and achieved 85% accuracy and 84% F1-score for anomaly detection. Diamanti *et al.* [18] used a modified CNN method, called look-behind fully CNN, on KID2 dataset for anomaly detection. They achieved 88.2% accuracy using 10-fold cross validation. Vasilakakis *et al.* [19] used a modified CNN for detecting anomalies on KID2 dataset in binary approach and achieved 90.0% AUC.
- Finally, there are few researches that targeted multiclass anomaly detection [20,21]. Mohammed *et al.* [20] used residual Long Short-Term Memory architecture for classifying 14 different anomalies and achieved 55.0% F1-score. Nawarathna *et al.* used textons dictionary with KNN to classify images to erythema, blood (bleeding), ulcer, erosion, polyp and normal and achieved 91.1% accuracy.

Despite advances in mentioned deep learning and machine learning approaches, the multiclass anomaly detection is still new, and more efforts can apply into it. Mohammed *et al.* [20] showed that increasing number of classes makes the problem more complicated and causes drop in performance. Furthermore, one of the most common issues with clinical datasets is data imbalance.

The main contribution of this work is to introduce a framework for multiclass classification on imbalance data using ensemble of deep OCC classifications that can perform classification with competitive accuracy. For multi-class and binary anomaly detection, one-class classification (OCC) has some merits over other methods.

- The OCC can concentrate on only one class and tend to conform to the corresponding target class. Therefore, the unique properties of a class can be captured while preventing over-fitting at the same time. This also helps better generalization [22].
- OCC is more suitable when other class is either absent, improperly sampled, or not correctly specified. Although the number of frames captured by WCE is huge, there are a few specific locations that have anomalies; therefore, the number of captured frames with anomaly are less than normal frames. This raises the imbalance issue which is popular in medical data [23]. For example, in KID2 dataset, there are 1,778 normal images while number of images with polyp is 44.
- When number of classes increases, the sophistication of a problem increases. Because the specification of decision boundaries becomes more complicated due to higher overlap. However,

dividing the problem to multiple binary classifiers, which is known as decomposition strategy, can break the problem to simpler sections that can be solved by any classifiers.

- For each OCC, the training process is independent and can thus be conveniently run in a parallel setting to minimize computing time [24].

As only one side of the boundary can be defined in OCC, it is difficult to ascertain how closely the boundary can match in any of the directions around the data on the basis of only one class. In this paper, we extracted features using an autoencoder technique, whose significance is shown in many feature extraction applications [25]. Moreover, for having better accuracy for OCC, we found that oversampling can help. Since, having well defined clusters is a challenge in OCC, we used Ordering Points to Identify the Clustering Structure (OPTICS), which does not require number of cluster and consider the density. Moreover, fine tuning parameters is applied using evolutionary optimization based on ant colony algorithm. The proposed algorithm is evaluated in two ways. One for detecting anomalies in binary form, which only need normal data, and another for classifying normal, inflammation, vascular and polyps' images, which is trained based on only normal, vascular and inflammation classes and an ensemble technique using XGBoost is used for aggregating OCCs.

The rest of this paper is organized as follows: in the next section, information about images and formulation of methods used in this study is presented. Section 3 provides the results of the proposed method. The discussion is provided in section 4, and the last section is the conclusion.

## 2. MATERIALS AND METHODS

### 2.1 Datasets

In this study, KID2 dataset is used which contains images captured by MiroCam capsule endoscope with 360×360 pixels resolution [26]. From KID2, 227 images of inflammatory abnormalities (aphthae, cobblestone mucosa, ulcers, luminal stenosis, mucosal/villous oedema, mucosal breaks with surrounding erythema and/or fibrotic strictures), 44 images of polyposis abnormalities (lymphoma, lymphoid nodular hyperplasia, Peutz-Jeghers polyps), 303 images with vascular issues (small bowel angiectasias and blood in the lumen), and 1,778 normal images were acquired from esophagus, stomach, small intestine and colon. The detailed description is provided in Table 1.

**TABLE 1.** Images used from each dataset

Dataset	Type	No. of images	Description
KID2	Normal	1,778	without anomaly and without specified locations
	Inflammation	227	aphthae, cobblestone mucosa, ulcers, luminal stenosis, mucosal/villous oedema, mucosal breaks with surrounding erythema and/or fibrotic strictures
	Vascular	303	small bowel angiectasias and blood in the lumen
	Polyps	44	lymphoma, lymphoid nodular hyperplasia, Peutz-Jeghers polyps

### 2.2 Proposed Method

The proposed algorithm has three main stages - preprocessing, feature extraction, and classification as

shown in Figure 1. A modified histogram equalization, based on Gamma Correction Extreme-Level Eliminating with Weighting Distribution, is used for preprocessing step. Then, the feature selection is performed using latent vector generated by training an autoencoder. Finally, an optimized Support Vector Data Descriptions (SVDD) is utilized for OCC on part of one class data and all SVDDs are ensemble for multiclass classification task. The steps are discussed in the following sections.

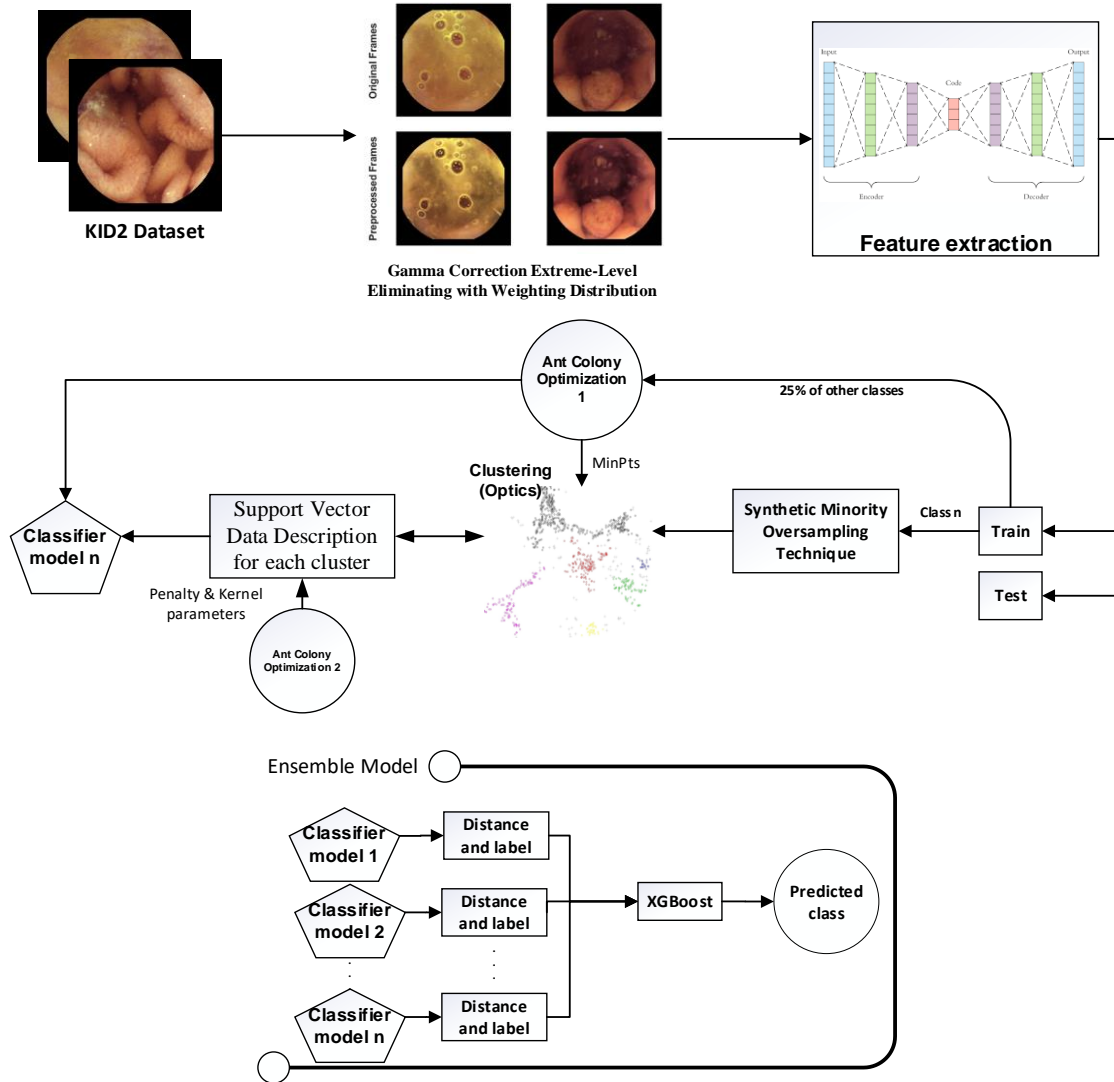


**FIGURE 1.** THE PROPOSED FRAMEWORK BASED ON ONE-CLASS CLASSIFICATION. FOR BINARY CLASSIFICATION, THE ENSEMBLE PART (BOTTOM BLOCK) THAT USES XGBOOST IS NOT REQUIRED.

### 2.2.1 Preprocessing

Since the capsule endoscopy images are registered with low light and low-resolution conditions, the resolution and quality of images should be improved before feature extraction. Some of the capsule endoscopic devices have monochrome camera chipset and color mapping is applied on captured luminance for creating Red (R), Green (G) and Blue (B) channels [27]. However, color channels may misalign together due to rapid movements which makes it difficult to extract robust features [28]. Furthermore, the capsule endoscopy devices are equipped with Light Emitting Diodes (LEDs) which leads to inhomogeneity in light saturation [29] and surfaces closer to the LEDs get more lights, hence, the illumination correction is a crucial step.

For preprocessing, a modified histogram equalization, namely as Gamma Correction Extreme-Level Eliminating with Weighting Distribution (GCELEWD) is applied on value channel (V) of HSV

color space [30], since  $V$  channel offers the benefit of classifying images based on information on brightness, which is equivalent to human visual perception and also used in similar researches [31]. The  $V$  channel has values between 0 and  $L$ . Two extreme levels are ignored and the Probability Density Function (PDF) is calculated, namely as  $\text{PDF}(V)$ . For flattening the enhancement, the Weighting Distribution Function (WDF) is defined as:

$$\text{PDF}_{\text{WDF}}(V) = \text{PDF}_{\text{max}} \left( \frac{\text{PDF}(V) - \text{PDF}_{\text{max}}}{\text{PDF}_{\text{max}} - \text{PDF}_{\text{min}}} \right)^\alpha \quad (1)$$

where  $\alpha \in [0,1]$ , and  $\text{PDF}_{\text{max}}$  and  $\text{PDF}_{\text{min}}$  are the maximum and minimum value of PDF, respectively. A blurred and darkened image can be generated with a low alpha value ( $\alpha$ ), whereas an over enhancement can be result of a high alpha value. The alpha value is set to 0.5 based on sigmoid function [30] and we used the same value. For histogram equalization, the transform function ( $\text{TF}(V_s)$ ) is required which is calculated based on cumulative density function (CDF):

$$\text{TF}(V_s) = \frac{\text{CDF}_n(V_s) + M_{V_s}^{1-\text{CDF}_n(V_s)}}{2} \quad (2)$$

where,  $\text{CDF}_n(V)$  is the normalized CDF of  $\text{PDF}_{\text{WDF}}(V)$ ,  $s$  is the normalized intensity level and  $V_s$  is normalized intensity level in channel  $V$ . After applying the proposed preprocessing, the image is converted back to RGB for feature extraction.

## 2.2.2 Feature extraction and over-sampling

### 2.2.2.1 Deep feature using convolutional autoencoder

For extracting deep features, two dimensional Convolution layers (Conv2D) are applied on RGB image along with the Leaky Rectified Linear Unit activation (LeakyReLU) function [32]. Three encoding layers based on Conv2D with filter size 7, 5 and 1 and kernel size 5 with activation function LeakyReLU are used. Then, a dense layer with size 26 is utilized in the next layer to get the latent vector. A similar architecture is used for decoding. The network is trained for training data on 100 epochs. For extracting features, only encoding layers are used for calculating latent vector as deep feature.

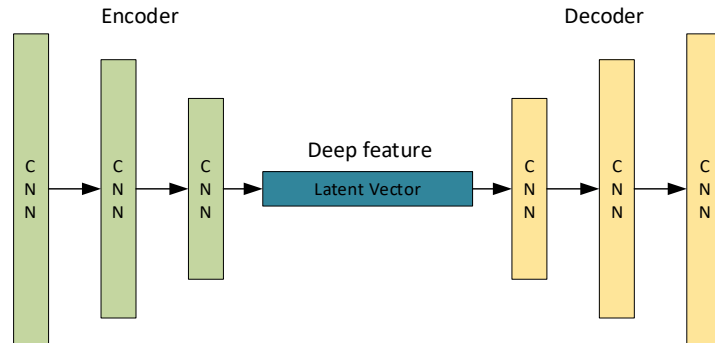


FIGURE 2. THE ARCHITECTURE OF THE DEEP FEATURE EXTRACTION METHOD

### 2.2.2.2 Over-sampling

The more images used for extracting features helps the clustering approach to cover the feature space better which leads to a more generalize model. Since, some classes are imbalance, we consider an over-sampling approach, called Synthetic Minority Over-sampling Technique (SMOTE) [33], wherein instead of oversampling with substitution, the features are oversampled by creating synthetic cases. For generating a synthetic sample, K-means clustering with five initial clusters are applied on feature space. Then in each cluster, the difference between a sample and its

nearest neighbor inside the cluster is calculated. This distance is multiplied by a random number between 0 and 1, and is applied to the proposed sample. This strategy essentially forces the decision-making area of SVDD to become more general. In this work, the over-sampling amount is set to 100%. This means that for each k-means cluster, 20% of samples are generated synthetically.

### 2.2.3 Clustering

The clustering of target data before applying OCC leads to several improvements compared with the typical OCC models:

- Boundary methods, such as SVDD, have better generalization abilities than clustering-based (reconstruction) OCC, however they are vulnerable to unusual data distributions. Therefore, a composite strategy using both methods incorporate the benefits of both while reducing their disadvantages.
- A SVDD classifier trained on a more lightweight data partition typically has a smaller number of support vectors.
- Since, each classifier is trained only on a subset of the data, its complexity is less of a single model method. This fact decreases the risk of overtraining and also leads to a substantial decrease in execution time.

The method called, Ordering Points to Identify the Clustering Structure (OPTICS) [34], has been shown to be appropriate for problems that have clusters with different dispersions across various density-based clustering algorithms. It does not require several runs on various pre-defined cluster numbers, unlike K-means or any other aggregative clustering process. There are two parameters required for the OPTICS algorithm, namely MinPts and  $\epsilon$ , which show the minimum number of points in the cluster and the Euclidean distance, respectively.

A point  $p$  is referred to a “core point” if number of points with distance smaller than  $\epsilon$  are at least MinPts [35]. If  $q$  is a core point and  $p$  is in its neighborhood with distance  $< \epsilon$ , point  $p$  is called directly density-reachable from point  $q$ . Point  $p$  is density-reachable from another point  $q$  if there is a sequence of points  $p_1, \dots, p_n$  where  $p_{i+1}$  can be reached directly from  $p_i$ , therefore  $p_1 = q$  and  $p_n = p$ . Each point in the dataset could be the core point if  $\epsilon$  parameter is set to the maximum distance between every point in the dataset. In this regard, the MinPts is the only parameter that should be set. Most similar points (AcSs) become neighbors in OPTICS. The first AcS is chosen as the current point in this process. Its Reachability Distance (RD) is set to Infinity (INF) and its closest neighbor is then set as the current point. Its RD is determined from the previous AcS as the smallest density reachable distance. This method is repeated until it processes all the points. Finally, the entire space of the feature is translated to a two-dimensional diagram wherein the x-axis relates to the ordered points and the RD of the ordered points is represented by the y-axis. Each RD valley is a potential cluster, with the point referring to the minimum RD in the valley becoming the corresponding representation of the cluster. The optimization is applied for selecting the appropriate MinPts.

### 2.2.4 One-class classification

There are four main categories for an OCC system. The density-based method, such as mixture of gaussian and Parzen density estimation, gets the distribution of target class [36]. However, this type of methods needs high number of examples. The reconstruction-based methods, such as autoencoder in neural networks, attempt to capture the structure of target class [37]. In boundary-based methods, such as SVDD and minimum spanning tree, the boundary enclosing the target class is predicted [38]. The key challenge of these approaches is to find the optimal size of the model enclosing the given training instances, as choosing a too small one will lead to an overtrained model, while a too large one contributes to an unnecessary inclusion of outliers into the target class. Finally, the ensemble-

based methods, such as one-class clustering based ensemble, utilize different classifier to cover whole target space [39]. In this paper, the SVDD is used as boundary-based component, auto-encoder for feature extraction as the reconstruction-based component and OPTICS clustering is used as ensemble-based parts for making a stronger OCC.

SVDD attempts to determine the minimum hypersphere which is containing as much as the desired data as possible while rejecting most of the feature space outliers [40]. The hypersphere can be defined simply by center  $\alpha$  and radius  $R$  and SVDD can be defined as following optimization problem:

$$F(R, \alpha) = R^2 + C \sum_i \xi_i \quad (5)$$

$$\text{subject to: } \|x_i - \alpha\|^2 \leq R^2 + \xi_i, \quad \xi_i \geq 0,$$

where,  $\xi_i$  denotes the error estimation of  $i$ -th sample,  $x_i$  is the  $i$ -th sample, and  $C$  is a penalty factor which can be used to regulate the number of bearable outliers. Using Lagrange Multipliers  $u_i \geq 0$  and  $v_i \geq 0$ , the equation 5 can be converted to Lagrangian  $L$ :

$$L = R^2 + C \sum_i \xi_i - \sum_i v_i (R^2 + \xi_i - \|x_i - \alpha\|^2) - \sum_i u_i \xi_i \quad (6)$$

By taking partial derivative respect to  $R$ ,  $\alpha$  and  $\xi_i$  and solving equations when they are equal to zero, the following equations are obtained:

$$\sum_i v_i = 1, \quad \alpha = \sum_i v_i x_i, \quad 0 \leq v_i \leq C \quad (7)$$

The last condition ( $0 \leq v_i \leq C$ ) means that data samples should be in the boundary of hypersphere which is called support vector. The dual optimization problem for equation 6 can be defined with help of equation 7 as:

$$L = \sum_i v_i \phi(x_i, x_i) - \sum_{i,j} v_i v_j \phi(x_i, x_j) \quad (8)$$

$$\text{subject to: } 0 \leq v_i \leq C \text{ and } \sum_i v_i = 1,$$

where,  $\phi(x_i, x_i)$  is the kernel function that can map data to higher dimensional space.

To test new sample  $y$ , its distance to the center of hypersphere should be calculated and if this distance is greater than  $R$ , the sample belongs to anomaly class:

$$\|y_i - \alpha\|^2 = \phi(y_i, y_i) - 2 \sum_i v_i \phi(y_i, x_i) + \sum_{i,j} v_i v_j \phi(x_i, x_j) \quad (9)$$

In this paper, Gaussian function  $\phi(x_1, x_2) = \exp(-\frac{\|x_1 - x_2\|^2}{2\sigma^2})$  is selected as kernel function since it can give a closed data description. The standard deviation of Gaussian kernel which defines kernel width, and penalty factor  $C$ , which indicates how many outliers beyond the boundaries may be assigned, are selected based on Ant Colony Optimization (ACO) [41,42]. It is worth noting that these parameters should be optimized for each cluster separately.

### 2.2.5 Ant Colony Optimization

ACO is a stochastic optimization technique which is inspired by the behavior of ants for finding their path from colony to food source [42]. In ACO, ants try to find the minimum cost path in problem space and help each other by pheromone trails in finding the optimum solution. ACO is essentially based on the process of creating new solutions where the  $n$  dimensional continuous optimization problem has  $n$  variables and in order to generate a variable, it is sampled from Gaussian distribution. The standard deviation of the Gaussian distribution is set by average distance between selected

solution and all other solutions. After the construction of new solutions, they are added to the initial solutions and sorted ascendingly based on objective function (updating pheromone) and some solutions are eliminated from the bottom to up until the number of solutions remain as it was in the first.

### 2.2.6 Training and evaluation

Concisely, the MinPts value for clustering, the standard deviation of Gaussian kernel for each cluster and the penalty factor  $C$  are parameters that need to be optimized. In this regard, two different ACO, which hereafter they called ACO1 and ACO2, are used. The ACO1 is used for finding the best MinPts and the second one is used for finding penalty factor and kernel parameter. The objective function of the ACO2 is same as equation 8. On the other hand, the objective function for ACO1 is maximizing F1-score which is described in Table 2. The termination criteria are met when there was no change after 7 steps or number of iterations is reached. The number of iterations for ACO1 and ACO2 is set to 100 and 1000, respectively. For limiting the problem space, the range of penalty factor  $C$  is set to  $[10^{-4}, 1]$ , the range of standard deviation of kernels is set to  $[10^{-4}, 10^2]$  and the range of MinPts is set from 5 to half of the training size. These ranges are selected based on trial and error and assumed to cover most of problem space.

In this paper, two different classifiers are trained and evaluated. First, all data are labeled as normal and abnormal and one model is trained only on normal data for anomaly detection. For the second classification model, three models are trained on normal, vascular and inflammatory data. Each model has two outputs. 1) A binary number indicates whether the input belongs to its class or not. 2) The minimum distance of the input against support vectors in clusters. These two outputs are ensembled from three models using XGBoost classifier [43] for multiclass classification problem. XGBoost classifier works based on boosting mechanism, wherein subsequent models are attempting to correct the error of the previous one by giving higher weight to inaccurate predictions. In this case, the weighted average of all models was used as the final model.

The pseudo code for anomaly detection is provided in Figure 3. Likewise, different binary classification models for other classes can be created and finally the ensemble of the results are used for multiclass classification.

<b>The pseudo code of the training procedure</b>
<b>Results:</b> A one-class classification model that can detect anomaly
<b>Step 1: Preprocessing:</b>
Convert color space to HSV
Calculate weighting distribution function using V channel
Transform V channel using transfer function
Convert HSV to RGB using new V channel
<b>Step 2: Extract latent vector as features based on autoencoder</b>
<b>Step 3: Training one-class classification model:</b>
Shuffle one of the classes data
Stratified partitioning 75% of the data for training, 25% for test set.
Until termination criteria of ACO1 are met, run the following steps:
Generate (next) ant's population for MinPts (ACO1)
Clustering training data using OPTICS
For each cluster:
Until termination criteria of ACO2 are met, run the following steps:
Generate (next) ant's population for $\sigma$ and $C$ (ACO2)
Optimize objective function SVDD (equation 6) for each cluster
Optimize F1-score for validation data on equation 7 and calculate F1-score

**FIGURE 3.** THE PSEUDO CODE FOR THE PROPOSED METHOD.

To have a consistent result, the whole algorithm is run 5 times with shuffling. Finally, the average

and standard deviation of performance metrics on test set is reported. The systematic performance metrics which are used in this research is shown in Table 2 [44]. For multiclass classification the average of measurement indices of one class against all is calculated.

**TABLE 2.** Indices for measuring the performance

Parameter	Definition	
	2-class	Multiclass (Macro Average)
Recall	$\frac{TP}{TP + FN}$	$\frac{1}{l} \sum_{i=1}^l \frac{TP_i}{TP_i + FN_i}$
Precision	$\frac{TP}{TP + FP}$	$\frac{1}{l} \sum_{i=1}^l \frac{TP_i}{TP_i + FP_i}$
F1-score	$\frac{2 \times \text{Recall} \times \text{Precision}}{\text{Recall} + \text{Precision}}$	$\frac{1}{l} \sum_{i=1}^l \frac{2 \times \text{Recall}_i \times \text{Precision}_i}{\text{Recall}_i + \text{Precision}_i}$
Accuracy	$\frac{TP + TN}{TP + TN + FP + FN}$	$\frac{\sum_{i=1}^l TP_i}{TP + TN + FN + FP}$

True positive ( $TP_i$ ): images belong to class  $i$  correctly classified; True negative ( $TN_i$ ): images do not belong to class  $i$  correctly classified; false positive ( $FP_i$ ): images do not belong to class  $i$  classified incorrectly as images in class  $i$ ; true negative ( $FN$ ): images belong to class  $i$  incorrectly identified as images in class;

### 3. RESULTS

#### 3.1. PREPROCESSING

For the preprocessing step, the GCELEWD algorithm is performed to improve contrast and brightness. The preprocessing step increases the entropy and contrast of images and makes the image intensity values spread better in each channel while considering their relative values to each other. The normalizing is applied before applying image to the deep neural network for feature extraction and the preprocessing helps the normalization to be centralized better. As an illustration, the logarithm of PDF for RGB channels and entropy of one frame before and after applying preprocessing step is provided in Figure 4.

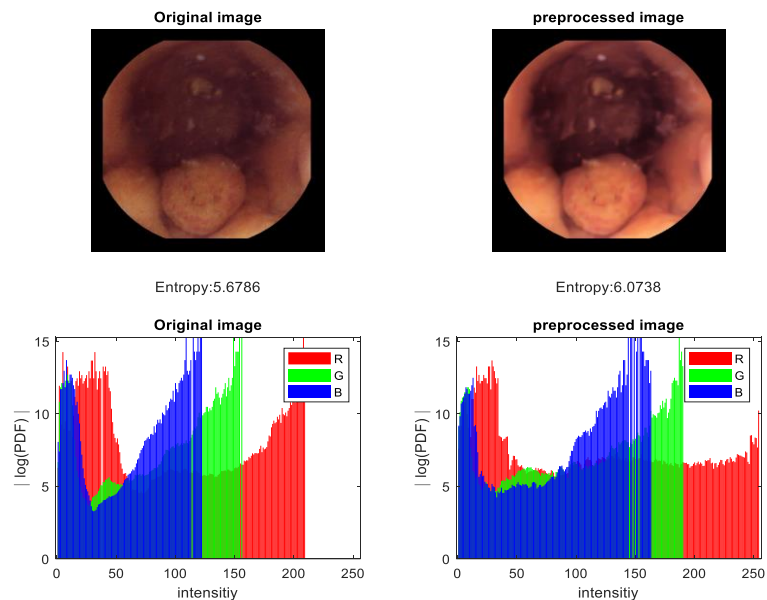


**FIGURE 4.** COMPARING ENTROPY AND HISTOGRAM OF A FRAME, BEFORE AND AFTER APPLYING PREPROCESSING. THE LOGARITHM OF PDF FOR RGB CHANNELS, RATHER THAN HISTOGRAM IS PROVIDED FOR BETTER COMPARISON.

### 3.2. CLASSIFICATION

Anomaly detection model consists of group of SVDDs that each one belongs to one cluster in normal data. This model is only trained on normal data and has not seen any abnormal images. Totally, 1333 normal images are used for training SVDDs with ACO1. The ACO2 also optimized F1-score for anomaly detection on 1333 normal and 430 abnormal images. The evaluation is performed on test set with 144 abnormal and 445 normal images. It is worth mentioning that anomaly detection does not need the ensemble classifier. The training procedure is performed 5 times, and each time, the normal data is shuffled. Using deep features, the average and standard deviation of accuracy, precision, recall and F1-score are  $94.9 \pm 0.3 \%$ ,  $94.9 \pm 0.3 \%$ ,  $97.7 \pm 0.3 \%$  and  $96.3 \pm 0.2 \%$ , respectively. The boxplot of precision, recall and F1-score for all five runs is depicted in Figure 6. It is worth to mention that since number of normal samples are enough, SMOTE can be removed with no effect on anomaly detection.

As mentioned in Table 1, the inflammation anomaly in the KID2 dataset consists of 227 images from ulcers, aphthae, mucosal breaks with surrounding erythema, cobblestone mucosa, luminal stenosis, fibrotic strictures, and mucosal/villous edema. On the other hand, the 303 vascular anomalies include small bowel angiectasias and blood in the lumen, and the polypoid images are selected from 44 images of KID2 which have nodular lymphoid hyperplasia, lymphoma, and Peutz-Jeghers polyps. For classifying images to specific anomaly categories, three models are trained. The model trained in previous step for detecting anomaly is selected as one of the models. Then, two distinct models are trained in a similar way, for inflammatory and vascular anomaly detection.

The training procedure is performed 5 times and each time the training data is shuffled. Using deep features, the average and standard deviation of accuracy, precision, recall and F1-score are  $94.8 \pm 0.4 \%$ ,  $82.6 \pm 0.5 \%$ ,  $87.6 \pm 0.5 \%$  and  $85.0 \pm 0.4 \%$ , respectively. The boxplot of precision, recall and F1-score for all five runs is depicted in Figure 5. Figure 6 shows the performance of the proposed method for each class in multiclass classification problem. Accuracy is weighted toward the dominant class because the data set is imbalanced, and it is not a proper performance index [45], therefore the F1-score is more important in multiclass classification.

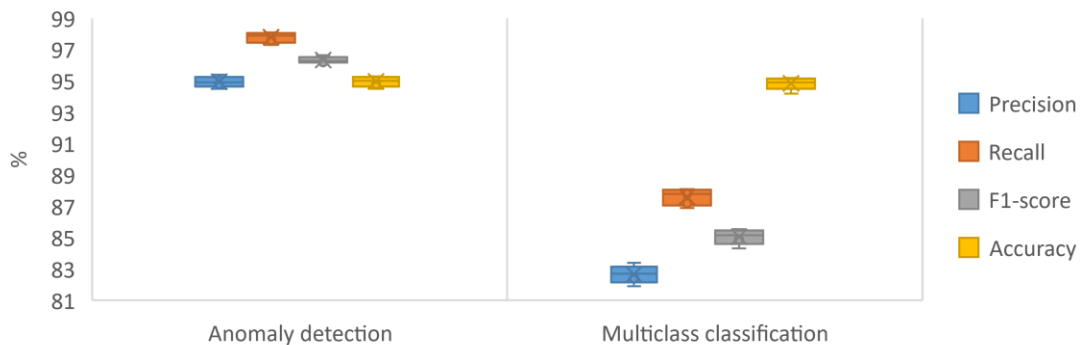


**FIGURE 5.** THE PERFORMANCE OF THE PROPOSED METHOD FOR ANOMALY DETECTION AND MULTICLASS CLASSIFICATION IN 5 TIMES RUNNING WITH SHUFFLING TRAINING DATA.

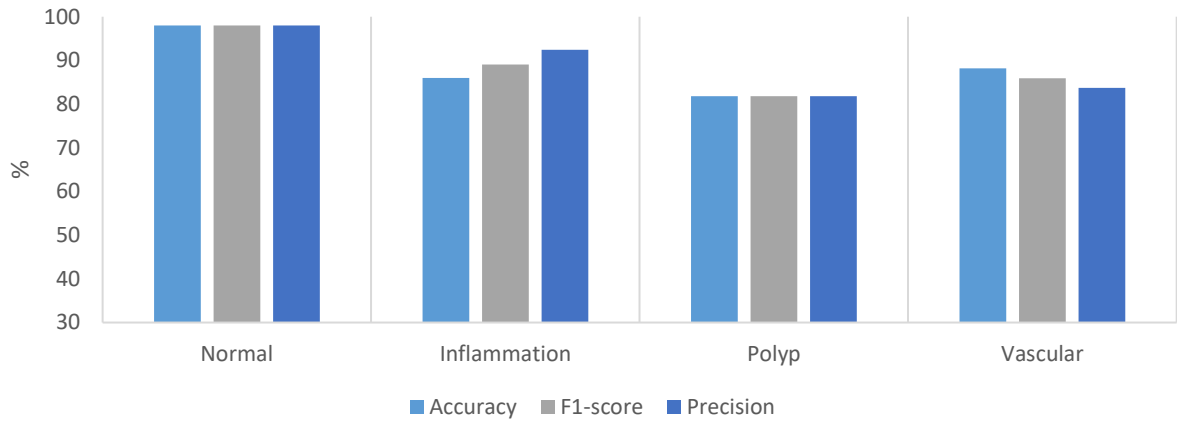


**FIGURE 6.** THE AVERAGE PERFORMANCE OF THE PROPOSED METHOD EACH CLASS ON MULTICLASS CLASSIFICATION. RECALL AND ACCURACY OF SINGLE CLASS ARE SAME.

#### 4. DISCUSSION

In this study, deep features learning is utilized based on combination of ACO, OPTICS and SVDD for anomaly detection and multiclass classification. Each step of the whole algorithm plays a significant role in acquired accuracy. The preprocessing step was crucial step since it could enhance the performance about 4% F1-score. The performance of anomaly detection and multiclass classification with and without preprocessing is depicted in Figure 7.

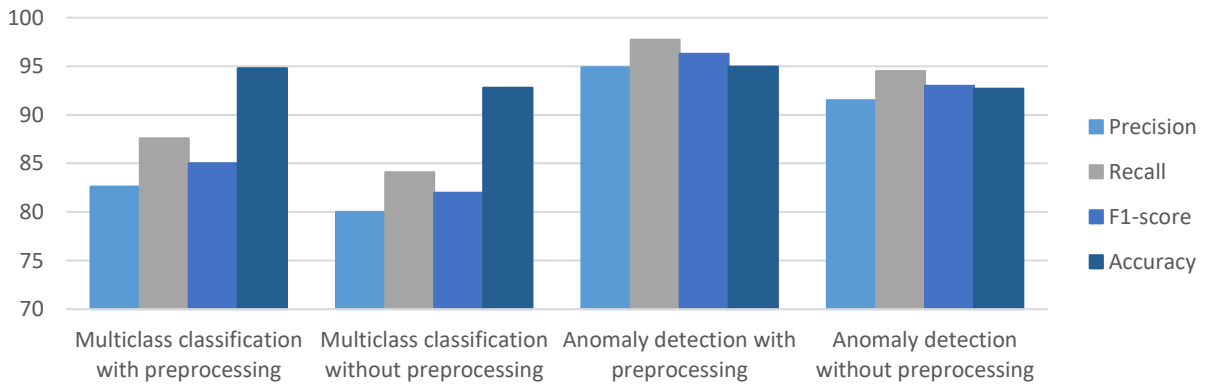


**FIGURE 7.** THE PERFORMANCE OF THE PROPOSED METHOD FOR ANOMALY DETECTION AND MULTICLASS CLASSIFICATION WITH AND WITHOUT PREPROCESSING.

Although images are normalized before applying deep feature extraction, the preprocessing step is a nonlinear map that change the input values to improve the entropy. Moreover, it is possible to use any other swarm optimization technique and for showing cases, we tested Genetic Algorithm (GA) [46] and Particle Swarm Optimization (PSO) [47]. However, the ACO requires less iteration which can reduce the training time. Nevertheless, all optimization techniques finally converge to a similar optimum point. The reason for choosing F1-score as fitness function is that it is robust to imbalanced data problems and can just be skewed from one way [48], wherein selecting the wrong objective or fitness function introduce bias towards the majority [49]. Figure 8 shows the convergence of the cost function in 100 iterations using ACO, GA and PSO.

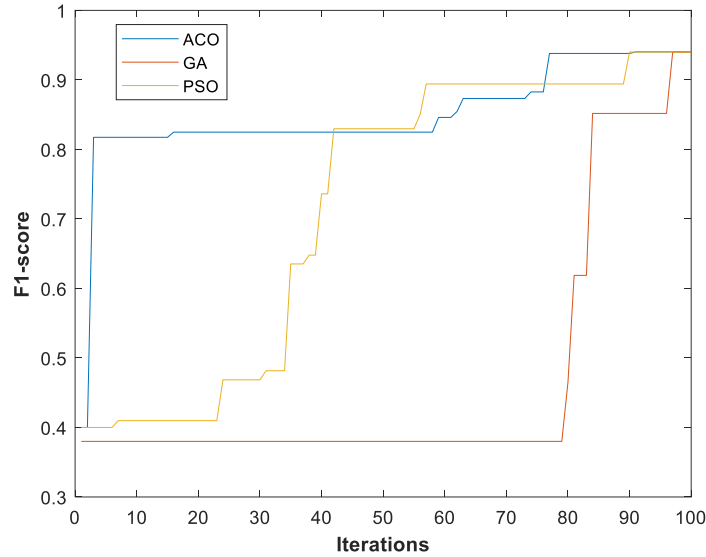


**FIGURE 8.** THE BEST F1-SCORE ACHIEVED BY ACO, GA AND PSO FOR DIFFERENT ITERATIONS. ACO CONVERGENCE RATE IS BETTER, BUT ALL ALGORITHMS ARE CONVERGED TO SAME OPTIMUM POINTS FINALLY.

One may ask that what is the performance of state-of-the-art deep learning approaches classification. It is worth noting that the number of training samples is very small, and not enough for training a perfect model in deep learning. To show the advantage of the proposed method, we applied transfer learning using GoogleNet, AlexNet, Resnet50 and VGG16 which are pretrained on ImageNet for comparison [50]. These models are used for anomaly detection, and from each class, 50% of data are used for training, 25% is set for validation and 25% is utilized as test set. Figure 9 shows the performance of the transfer learning models compared with the proposed method. The proposed method achieved 12.3% and 15% F1-score improvement over GoogleNet and Resnet50 as the best transfer learning methods for anomaly detection and multiclass classification, respectively. One of the possible reasons is that the transfer learning methods are pretrained on ImageNet which were taken mostly from natural scenes.

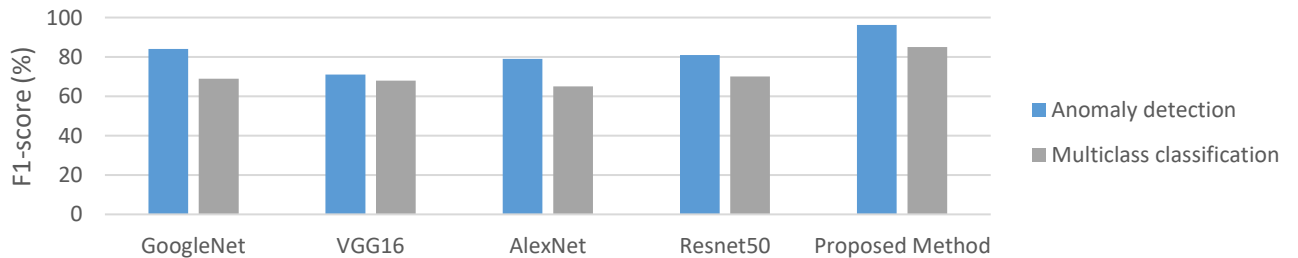


**FIGURE 9.** COMPARING STATE-OF-THE-ART CLASSIFICATION ALGORITHM WITH PROPOSED METHOD. THE PROPOSED METHODS ARE BASED ON SEMI-SUPERVISED LEARNING WHILE OTHERS ARE SUPERVISED LEARNING.

There have been several works on computer-aided decision support schemes to improve effectiveness and diagnostic accuracy for anomaly detection as well as classifications. Table 3 provides a comparison between several relevant techniques from the literature and the proposed method.

**TABLE 3.** COMPARISON BETWEEN THE PROPOSED METHOD AND RECENT APPROACHES.

Article Cited	Detected output	Binary or Multiclass(#classes)	Dataset	Validation strategy (number of frames for total /test)	Method	Performance in %, index
[10]	Polyp	Binary	PA [11]	hold-out (270/30)	Inpainting diffusion algorithm combined with energy map	84.2 Accuracy

(Zhou et al., 2014)	Polyp	Binary	Private	hold-out (294/65)	Variance of color channels with SVM	90.7 Accuracy
[14]	Polyp	Binary	Private	Five times hold-out with shuffling (1930/150)	Transfer learning for feature extraction and SVM for classification	87.0 F1-score 85.9 Accuracy
[12]	Polyp	Binary	Private	External dataset (73)	KoloPol APDS software	85.3 Accuracy
[51]	Polyp	Binary	Private	hold-out (2684/338)	GI-Genius, Medtronic software	82.0 accuracy
[16]	Inflammatory	Binary	KID1 [15]	hold-out (400/54)	CNN	90.2 Accuracy
(Ševo et al., 2016)	Inflammatory	Binary	Private	External dataset (231)	Edge and texture analysis	84.0 Accuracy
[18]	Anomaly	Binary	KID2	10-fold (2352)	Look-Behind Fully CNN	88.2 Accuracy
[17]	Anomaly	Binary	KID1 and KID2	5-fold (2448)	Random forest-based ensemble classifier with fractal features	85.0 Accuracy 84.0 F1-score
[19]	Anomaly	Binary	KID2	10-fold (2352)	multi-scale and multi-label CNN	90.0 AUC
[21]	Anomaly (erythema, blood, ulcer, erosion, and polyp)	Multiclass (6)	Private	10-fold (1750)	Textons dictionary with KNN	91.1 Accuracy
[20]	Anomaly (14 different anomalies)	Multiclass (14)	Private	hold-out (28304/14152)	Residual LSTM	55.0 F1-score
<b>Proposed method</b>	Anomaly (Inflammatory and Polyp, vascular)	Multiclass (4)	KID2	Five times hold-out with shuffling (2352/ 588)	Optimized OCC	<b>85.0 F1-score</b> <b>94.8 Accuracy</b> <b>87.2 Recall</b>
<b>Proposed method</b>	Anomaly	Binary	KID2	Five times hold-out with shuffling (2352/ 588)	Optimized OCC	<b>96.3 F1-score</b> <b>94.9 Accuracy</b> <b>97.7 Recall</b>

PA: Publicly available; NA: Not available; hold-out (total size/ test size); External dataset (total size); k-fold (total size);

Concisely, the proposed method could achieve the best F1-score and accuracy for anomaly detection among others. Most of the method did not train a model for multiclass classification. The other two methods that have multiclass classification has less accuracy or F1-score and are only applied on a private dataset which we could not apply the proposed algorithm on it. The average time of training the proposed algorithm using a computer with Intel Core i9-9900 3.6 GHz CPU and 16 GB of RAM is  $4471 \pm 453$  seconds. Training the model for extracting deep features takes  $1338 \pm 271$  seconds with CPU. On the other hand, the average time of applying proposed method on one frame is 146 ms. The trained system can be considered real-time for WCE, which usually has a frame rate less than 5 frames per second. All data processing and statistical analysis are performed on MATLAB (The Math Works Inc, Natick, MA, USA).

Further investigation and testing of the proposed method on large datasets are required for making a more general and robust tool. Furthermore, instead of having multi-step framework, the gradient algorithm can be utilized to optimized whole networks. However, there are some parts, such as clustering and oversampling, that currently are not currently differentiable. Another point is that kernels mostly used for support vector data descriptors are gaussian, linear, and polynomial and investigating other kernels such as genetic kernel [52] has potential of improving the performance.

## 5. CONCLUSION

An ensemble of one-class classifiers (OCC) is created for multiclass classification of anomalies in endoscopy. Each OCC is designed based on boundary-based and ensemble-based approach with the help of OPTICS clustering and Support Vector Data Descriptors which is optimized and tuned by Ant Colony Optimization. The key benefit of the proposed approach is that the combination of classifiers trained on

the basis of clusters allow us to leverage individual classifier advantages. The proposed method is applied on KID2 dataset for anomaly detection and anomaly type identification, wherein the images were highly imbalance respecting to others. The binary (OCC) and multiclass (ensemble) classifier could achieve  $96.3 \pm 0.2\%$  for detecting anomaly and  $85.0 \pm 0.4\%$  F1-score for classifying anomaly types, respectively. The proposed method outperforms transfer learning and other methods, and can therefore be used for classification problem that suffer from the data imbalance issue.

## 6. ACKNOWLEDGEMENT

Authors like to acknowledge funding from Natural Sciences and Engineering Research Council of Canada (NSERC) to support the work.

## REFERENCES

- [1] D.A. Schwartz, M.J. Wiersema, K.M. Dudiak, J.G. Fletcher, J.E. Clain, W.J. Tremaine, A.R. Zinsmeister, I.D. Norton, L.A. Boardman, R.M. Devine, A comparison of endoscopic ultrasound, magnetic resonance imaging, and exam under anesthesia for evaluation of Crohn's perianal fistulas, *Gastroenterology*. 121 (2001) 1064–1072.
- [2] D.S. Early, T. Ben-Menachem, G.A. Decker, J.A. Evans, R.D. Fanelli, D.A. Fisher, N. Fukami, J.H. Hwang, R. Jain, T.L. Jue, Appropriate use of GI endoscopy, *Gastrointest. Endosc.* 75 (2012) 1127–1131.
- [3] G. Ciuti, A. Menciassi, P. Dario, Capsule endoscopy: from current achievements to open challenges, *IEEE Rev. Biomed. Eng.* 4 (2011) 59–72.
- [4] T. Kuiper, W.A. Marsman, J.M. Jansen, E.J. van Soest, Y.C. Haan, G.J. Bakker, P. Fockens, E. Dekker, Accuracy for optical diagnosis of small colorectal polyps in nonacademic settings, *Clin. Gastroenterol. Hepatol.* 10 (2012) 1016–1020.
- [5] S. Yang, C. Lemke, B.F. Cox, I.P. Newton, I. N athke, S. Cochran, A Learning Based Microultrasound System for the Detection of Inflammation of the Gastrointestinal Tract, *IEEE Trans. Med. Imaging*. (2020) 1–1. <https://doi.org/10.1109/TMI.2020.3021560>.
- [6] T. Aoki, A. Yamada, K. Aoyama, H. Saito, A. Tsuboi, A. Nakada, R. Niikura, M. Fujishiro, S. Oka, S. Ishihara, T. Matsuda, S. Tanaka, K. Koike, T. Tada, Automatic detection of erosions and ulcerations in wireless capsule endoscopy images based on a deep convolutional neural network, *Gastrointest. Endosc.* 89 (2019) 357–363.e2. <https://doi.org/10.1016/j.gie.2018.10.027>.
- [7] S. Syed, R.W. Stidham, Potential for Standardization and Automation for Pathology and Endoscopy in Inflammatory Bowel Disease, *Inflamm. Bowel Dis.* 26 (2020) 1490–1497. <https://doi.org/10.1093/ibd/izaa211>.
- [8] M. Liedlgruber, A. Uhl, Computer-aided decision support systems for endoscopy in the gastrointestinal tract: a review, *IEEE Rev. Biomed. Eng.* 4 (2011) 73–88.
- [9] B.-P. Li, M.Q.-H. Meng, Comparison of Several Texture Features for Tumor Detection in CE Images, *J. Med. Syst.* 36 (2012) 2463–2469. <https://doi.org/10.1007/s10916-011-9713-2>.
- [10] J. Bernal, J. S anchez, F. Vilari no, Impact of image preprocessing methods on polyp localization in colonoscopy frames, in: 2013 35th Annu. Int. Conf. IEEE Eng. Med. Biol. Soc. EMBC, 2013; pp. 7350–7354. <https://doi.org/10.1109/EMBC.2013.6611256>.
- [11] J. Bernal, J. S anchez, F. Vilari no, Towards automatic polyp detection with a polyp appearance model, *Best Pap. Iber. Conf. Pattern Recognit. Image Anal. IbPRIA2011*. 45 (2012) 3166–3182. <https://doi.org/10.1016/j.patcog.2012.03.002>.
- [12] P. Klare, C. Sander, M. Prinzen, B. Haller, S. Nowack, M. Abdelhafez, A. Poszler, H. Brown, D. Wilhelm, R.M. Schmid, S. von Delius, T. Wittenberg, Automated polyp detection in the colorectum: a prospective study (with videos), *Gastrointest. Endosc.* 89 (2019) 576–582.e1. <https://doi.org/10.1016/j.gie.2018.09.042>.
- [13] S. Gulati, M. Patel, A. Emmanuel, A. Haji, B. Hayee, H. Neumann, The future of endoscopy: Advances in endoscopic image innovations, *Dig. Endosc.* 32 (2020) 512–522. <https://doi.org/10.1111/den.13481>.
- [14] R. Zhang, Y. Zheng, T.W.C. Mak, R. Yu, S.H. Wong, J.Y.W. Lau, C.C.Y. Poon, Automatic Detection and Classification of Colorectal Polyps by Transferring Low-Level CNN Features From Nonmedical Domain, *IEEE J. Biomed. Health Inform.* 21 (2017) 41–47. <https://doi.org/10.1109/JBHI.2016.2635662>.
- [15] A. Koulaouzidis, KID: Koulaouzidis-Iakovidis database for capsule endoscopy, 2016.
- [16] S.V. Georgakopoulos, D.K. Iakovidis, M. Vasilakakis, V.P. Plagianakos, A. Koulaouzidis, Weakly-supervised convolutional learning for detection of inflammatory gastrointestinal lesions, in: *IEEE*, 2016; pp. 510–514.
- [17] S. Jain, A. Seal, A. Ojha, O. Krejcar, J. Bureš, I. Tachec ı, A. Yazidi, Detection of abnormality in wireless capsule endoscopy images using fractal features, *Comput. Biol. Med.* 127 (2020) 104094. <https://doi.org/10.1016/j.combiomed.2020.104094>.
- [18] D.E. Diamantis, D.K. Iakovidis, A. Koulaouzidis, Look-behind fully convolutional neural network for computer-aided endoscopy, *Biomed. Signal Process. Control.* 49 (2019) 192–201. <https://doi.org/10.1016/j.bspc.2018.12.005>.

- [19] M.D. Vasilakakis, D. Diamantis, E. Spyrou, A. Koulaouzidis, D.K. Iakovidis, Weakly supervised multilabel classification for semantic interpretation of endoscopy video frames, *Evol. Syst.* (2018) 1–13.
- [20] A. Mohammed, I. Farup, M. Pedersen, S. Yildirim, Ø. Hovde, PS-DeVCEM: Pathology-sensitive deep learning model for video capsule endoscopy based on weakly labeled data, *Comput. Vis. Image Underst.* 201 (2020) 103062.
- [21] R. Nawarathna, J. Oh, J. Muthukudage, W. Tavanapong, J. Wong, P.C. De Groen, S.J. Tang, Abnormal image detection in endoscopy videos using a filter bank and local binary patterns, *Neurocomputing.* 144 (2014) 70–91.
- [22] B. Hadjadji, Y. Chibani, Y. Guerbai, Multiple one-class classifier combination for multi-class classification, in: 2014 22nd Int. Conf. Pattern Recognit., IEEE, 2014: pp. 2832–2837.
- [23] M.M. Rahman, D.N. Davis, Addressing the class imbalance problem in medical datasets, *Int. J. Mach. Learn. Comput.* 3 (2013) 224.
- [24] T. Wilk, M. Woźniak, Complexity and multithreaded implementation analysis of one class-classifiers fuzzy combiner, in: *Int. Conf. Hybrid Artif. Intell. Syst.*, Springer, 2011: pp. 237–244.
- [25] N. Lv, C. Chen, T. Qiu, A.K. Sangaiah, Deep learning and superpixel feature extraction based on contractive autoencoder for change detection in SAR images, *IEEE Trans. Ind. Inform.* 14 (2018) 5530–5538.
- [26] A. Koulaouzidis, D.K. Iakovidis, D.E. Yung, E. Rondonotti, U. Kopylov, J.N. Plevris, E. Toth, A. Eliakim, G.W. Johansson, W. Marlicz, KID Project: an internet-based digital video atlas of capsule endoscopy for research purposes, *Endosc. Int. Open.* 5 (2017) E477–E483.
- [27] B. Münzer, K. Schoeffmann, L. Böszörményi, Content-based processing and analysis of endoscopic images and videos: A survey, *Multimed. Tools Appl.* 77 (2018) 1323–1362. <https://doi.org/10.1007/s11042-016-4219-z>.
- [28] M. Arnold, A. Ghosh, S. Ameling, G. Lacey, Automatic segmentation and inpainting of specular highlights for endoscopic imaging, *EURASIP J. Image Video Process.* 2010 (2010) 1–12.
- [29] O.V. Hernández Mondragón, R. Zamarripa Mottú, O. Solórzano Pineda, R.A. Gutierrez Aguilar, L.F. García Contreras, Feasibility of using an led-probe in third-space endoscopy: a clinical study, *BMC Gastroenterol.* 20 (2020) 132. <https://doi.org/10.1186/s12876-020-01260-9>.
- [30] V. Teh, K.S. Sim, E.K. Wong, Contrast enhancement of CT brain images using gamma correction adaptive extreme-level eliminating with weighting distribution, *Int. J. Innov. Comput. Inf. Control.* 14 (2018) 1029–1041.
- [31] G. Palanisamy, N.B. Shankar, P. Ponnusamy, V.P. Gopi, A hybrid feature preservation technique based on luminosity and edge based contrast enhancement in color fundus images, *Biocybern. Biomed. Eng.* 40 (2020) 752–763.
- [32] P. Perera, R. Nallapati, B. Xiang, Ocgan: One-class novelty detection using gans with constrained latent representations, in: *Proc. IEEE Conf. Comput. Vis. Pattern Recognit.*, 2019: pp. 2898–2906.
- [33] N.V. Chawla, K.W. Bowyer, L.O. Hall, W.P. Kegelmeyer, SMOTE: synthetic minority over-sampling technique, *J. Artif. Intell. Res.* 16 (2002) 321–357.
- [34] J.C. Dassun, A. Reyes, H. Yokoyama, M. Dolendo, Ordering Points to Identify the Clustering Structure Algorithm in Fingerprint-Based Age Classification, *Virtutis Incunabula.* 2 (2015) 17–27.
- [35] M.R. Mohebian, H.R. Marateb, S. Karimimehr, M.A. Mañanas, J. Kranjec, A. Holobar, Non-invasive decoding of the motoneurons: A guided source separation method based on convolution kernel compensation with clustered initial points, *Front. Comput. Neurosci.* 13 (2019) 14.
- [36] S. Sonnenburg, G. Rätsch, C. Schäfer, B. Schölkopf, Large scale multiple kernel learning, *J. Mach. Learn. Res.* 7 (2006) 1531–1565.
- [37] C. Bellinger, S. Sharma, O.R. Zaiane, N. Japkowicz, Sampling a longer life: Binary versus one-class classification revisited, in: *First Int. Workshop Learn. Imbalanced Domains Theory Appl.*, PMLR, 2017: pp. 64–78.
- [38] M. Bicego, M.A. Figueiredo, Soft clustering using weighted one-class support vector machines, *Pattern Recognit.* 42 (2009) 27–32.
- [39] B. Krawczyk, M. Woźniak, B. Cyganek, Clustering-based ensembles for one-class classification, *Inf. Sci.* 264 (2014) 182–195.
- [40] M. Turkoz, S. Kim, Y. Son, M.K. Jeong, E.A. Elsayed, Generalized support vector data description for anomaly detection, *Pattern Recognit.* 100 (2020) 107119.
- [41] Q. Yang, W. Chen, Z. Yu, T. Gu, Y. Li, H. Zhang, J. Zhang, Adaptive Multimodal Continuous Ant Colony Optimization, *IEEE Trans. Evol. Comput.* 21 (2017) 191–205. <https://doi.org/10.1109/TEVC.2016.2591064>.
- [42] M. Dorigo, L.M. Gambardella, Ant colony system: a cooperative learning approach to the traveling salesman problem, *IEEE Trans. Evol. Comput.* 1 (1997) 53–66.
- [43] T. Chen, C. Guestrin, Xgboost: A scalable tree boosting system, in: *Proc. 22nd Acm Sigkdd Int. Conf. Knowl. Discov. Data Min.*, 2016: pp. 785–794.
- [44] M. Sokolova, G. Lapalme, A systematic analysis of performance measures for classification tasks, *Inf. Process. Manag.* 45 (2009) 427–437.
- [45] M. Mansourian, H.R. Marateb, M. Mansourian, M.R. Mohebbian, H. Binder, M.Á. Mañanas, Rigorous performance assessment of computer-aided medical diagnosis and prognosis systems: a biostatistical perspective on data mining, (n.d.).
- [46] S. Mirjalili, Genetic algorithm, in: *Evol. Algorithms Neural Netw.*, Springer, 2019: pp. 43–55.
- [47] R. Poli, J. Kennedy, T. Blackwell, Particle swarm optimization, *Swarm Intell.* 1 (2007) 33–57.
- [48] J.M. Johnson, T.M. Khoshgoftaar, Survey on deep learning with class imbalance, *J. Big Data.* 6 (2019) 27.

- [49] Y. Jin, A comprehensive survey of fitness approximation in evolutionary computation, *Soft Comput.* 9 (2005) 3–12.
- [50] S.J. Pan, Q. Yang, A survey on transfer learning, *IEEE Trans. Knowl. Data Eng.* 22 (2009) 1345–1359.
- [51] C. Hassan, M.B. Wallace, P. Sharma, R. Maselli, V. Craviotto, M. Spadaccini, A. Repici, New artificial intelligence system: first validation study versus experienced endoscopists for colorectal polyp detection, *Gut.* 69 (2020) 799. <https://doi.org/10.1136/gutjnl-2019-319914>.
- [52] T. Howley, M.G. Madden, An evolutionary approach to automatic kernel construction, in: *Int. Conf. Artif. Neural Netw.*, Springer, 2006: pp. 417–426.